Supporting Information

Highly Stable and Differentially Arranged Hexanuclear Lanthanide Clusters: Structure, Assembly Mechanism, and Magnetic Resonance Imaging

Wen-Wen Qin,[a] Yun-Lan Li,[a] Zhong-Hong Zhu,[a,*] Fu-Pei Liang,[a] Qiong Hu,[b,*] Hua-Hong Zou[a,*]

[a]School of Chemistry and Pharmaceutical Sciences, State Key Laboratory for Chemistry and Molecular Engineering of Medicinal Resources, Guangxi Normal University, Guilin 541004, P. R. China *E-mail (Corresponding author): 18317725515@163.com (Z.-H. Zhu), gxnuchem@foxmail.com (H.-H. Zou).

[b]Guangxi Key Laboratory of Agricultural Resources Chemistry and Biotechnology, College of Chemistry and Food Science, Yulin Normal University, Yulin 537000, P. R. China *E-mail (Corresponding author): huqiongscut@163.com (Q. Hu).

Keywords: Lanthanide cluster; Assembly mechanism; Solvothermal synthesis; Precise synthesis; Magnetic properties

Table of Contents:

Experimental Section

Materials and Measurements.

All reagents were obtained from commercial sources and used without further purification. Elemental analyses for C, H and O were performed on a varia MICRO cube. The infrared spectra were carried out on a Pekin-Elmer Two spectrophotometer with pressed KBr pellets. The powder X-ray diffraction (PXRD) spectra were measured on a Rigaku D/Max-3c diffractometer with Mo Kα radiation (λ = 0.71073 Å). Thermogravimetric analyses were performed on a PerkinElmer PyrisDiamond TG-DTA instrument under an N_2 atmosphere using a heating rate of 5 °C min^{-1} from room temperature up to 1000 °C. Magnetic properties were performed on a Superconducting Quantum Interference Device (SQUID) magnetometer. The diamagnetism of all constituent atoms was corrected with Pascal's constant.

Single crystal X-ray crystallography.

Diffraction data for the complex were collected on a ROD, Synergy Custom DW system, HyPix diffractometer (Mo-Kα radiation and λ = 0.71073 Å) in Φ and ω scan modes. The structures were solved by direct methods, and refined by a full-matrix least-squares method on the basis of F^2 by using SHELXL and OLEX2.[1] Anisotropic thermal parameters were applied to all non-hydrogen atoms. Hydrogen atoms were generated geometrically. The crystallographic data for **Dy_6 and HNP-Dy_6** are listed in Table S1, and selected bond lengths and angles are given in Table S2 and S3. The CCDC reference numbers for the crystal structures of **Dy_6** and **HNP-Dy_6** are 2283643 and 2283644.

HRESI-MS measurement.

HRESI-MS measurements were conducted at a capillary temperature of 275 °C. Aliquots of the solution were injected into the device at 2 μL. The mass spectrometer used for the measurements was a ThermoExactive and the data were collected in positive and negative ion modes. The spectrometer was previously calibrated with the standard tune mix to give a precision of *ca*. 2 ppm. within the region of m/z = 200−4000. The capillary voltage was 50 V, the tube lens voltage was 150 V, and the skimmer voltage was 25 V.

[1] Sheldrick, G. M. *Acta Crystallogr., Sect. C: Struct. Chem*. **2015**, *71*, 3−8.

The synthesis method.

Synthesis of H_2L^1 (N'^2,N'^6-bis(4-(diethylamino)-2-hydroxybenzylidene)pyridine-2,6-dicarbohydrazide): Pyridine-2,6-dicarbohydrazide (5 mmol, 0.976 g) was taken in a 50 mL round-bottomed flask and dissolved in 40 mL of ethanol and stirred for 30 min. 4-(*N*,*N*-Diethylamino)salicylaldehyde (10 mmol, 1.93 g) was added in portions to the aforesaid solution of pyridine-2,6-dicarbohydrazide. To this, two drops of concentrated sulfuric acid was added and the solution refluxed for 12 h. The resulting yellow solid (2.10 g, 76.92%) was filter under vacuum, washed methanol followed by drying under reduced pressure.

Synthesis of H_2L^2 (N'^2,N'^6-bis((2-hydroxynaphthalen-1-yl)methylene)pyridine-2,6-dicarbohydrazide): Pyridine-2,6-dicarbohydrazide (5 mmol, 0.976 g) was taken in a 50 mL round-bottomed flask and dissolved in 40 mL of ethanol and stirred for 30 min. 2-Hydroxy-1-naphthaldehyde (10 mmol, 1.72 g) was added in portions to the aforesaid solution of pyridine-2,6-dicarbohydrazide. To this, two drops of concentrated sulfuric acid was added and the solution refluxed for 12 h. The resulting yellow solid (1.92 g, 73.80%) was filter under vacuum, washed methanol followed by drying under reduced pressure.

Synthesis of Dy_6: A mixture of H_2L^1 (0.05 mmol, 27.3 mg), 0.4 mmol $Dy(OAc)_3{\cdot}4H_2O$ (approximately 165 mg), and triethylamine (100 μL) were dissolved in mixed solvent (CH_3OH:H_2O = 1.0 mL:0.3 mL) in a Pyrex tube. The tube was sealed and heated at 80 °C in an oven for 2 days, orange crystals were observed with a yield of about 45% (based on $Dy(OAc)_3{\cdot}4H_2O$). Elemental analysis theoretical value ($C_{70}H_{92}Dy_6N_{14}O_{28}$): C, 32.94%; H, 3.63%; N, 7.68%; experimental value: C, 32.82%; H, 3.51%; N, 7.56%. Infrared spectrum data (IR, KBr pellet, cm^{-1}): 3429 (m), 2970 (m), 1600 (s), 1565 (s), 1432 (w), 1136 (s), 1077 (s), 829 (m), 758 (m).

Synthesis of Gd_6: A mixture of H_2L^1 (0.05 mmol, 27.3 mg), 0.4 mmol $Gd(OAc)_3{\cdot}H_2O$ (approximately 141 mg), and triethylamine (100 μL) were dissolved in mixed solvent (CH_3OH:H_2O = 1.0 mL:0.3 mL) in a Pyrex tube. The tube was sealed and heated at 80 °C in an oven for 2 days, orange crystals were observed with a yield of about 44% (based on $Gd(OAc)_3{\cdot}H_2O$). Infrared spectrum data (IR, KBr pellet, cm^{-1}): 3429 (m), 2970 (m), 1601 (s), 1568 (s), 1431 (w), 1138 (s), 1077 (s), 829 (m), 758 (m).

Synthesis of HNP-Dy_6: A mixture of H_2L^2 (0.05 mmol, 25.2 mg), 0.4 mmol $Dy(OAc)_3{\cdot}4H_2O$ (approximately 165 mg), and triethylamine (100 μL) were dissolved in 2.0 mL of CH_3OH in a Pyrex

tube. The tube was sealed and heated at 80 °C in an oven for 2 days, yellow crystals were observed with a yield of about 40% (based on $Dy(OAc)_3 \cdot 4H_2O$). Elemental analysis theoretical value ($C_{76}H_{94}Dy_6N_{10}O_{34}$): C, 34.22%; H, 3.53%; N, 5.25%; experimental value: C, 34.06%; H, 3.47%; N, 5.16%. Infrared spectrum data (IR, KBr pellet, cm^{-1}): 3429 (m), 1601 (s), 1384 (s), 1350 (s), 1200 (m), 827 (m), 752 (s).

Solution MRI imaging experiments.

Gd_6: Prepare 1 mL of **Gd_6** solution with a concentration of 23.5 μM (the content of DMSO is less than 1%, which is used for solubilization). After conversion of results (**Gd_6**:Gd(III) ions = 1:6), the molar concentration of Gd(III) ions in the above-mentioned **Gd_6** mother liquor was obtainedas 141.0 μM. For solution MRI imaging experiments, the above-mentioned solutions containing Gd(III) ions at a concentration of 141.0 μM were diluted to 0.11, 0.23, 0.35, 0.47, 0.59 and 0.71 μM, respectively.

Table S1. Crystallographic data of the clusters **Dy_6** and **HNP-Dy_6**.

	Dy_6	**HNP-Dy_6**
Empirical formula	$C_{70}H_{92}Dy_6N_{14}O_{28}$	$C_{76}H_{94}Dy_6N_{10}O_{34}$
Formula weight	2550.95	2664.98
T, K	295 K	296 K
Crystal system	triclinic	triclinic
Space group	*P*-1	*P*-1
a, Å	10.2039(1)	11.4673(8)
b, Å	11.9012(1)	14.0210(7)
c, Å	19.2989(2)	14.7578(6)
α, °	86.127	106.670
β, °	86.641	90.919
γ, °	67.183	96.016
V, Å^3	2153.97(4)	2257.9(2)
Z	1	1
D_c, g cm^3	1.967	1.960
μ, mm^{-1}	27.97	26.76
F(000)	1229	1287
2*θ* range for data collection/°	4.592 to 133.198	6.26 to 153.3
Reflns coll.	23012	35481
Unique reflns	7591	8747
R_{int}	0.0896	0.1266
R_1[a] ($I > 2\sigma(I)$)	0.0957	0.1098
wR_2[b] (all data)	0.2661	0.3115
GOF	1.049	1.090

[a]$R_1 = \Sigma||F_o|-|F_c||/\Sigma|F_o|$, [b]$wR_2 = [\Sigma w(F_o^2-F_c^2)^2/\Sigma w(F_o^2)^2]^{1/2}$

Table S2. Selected bond lengths (Å) and angles (°) of cluster **Dy_6**.

Bond lengths (Å)					
Dy1-O4	2.195(10)	Dy2-O13	2.338(8)	Dy3-O10	2.303(10)
Dy1-O14	2.249(11)	Dy2-O6	2.344(10)	Dy3-O1	2.315(9)
Dy1-O7	2.290(10)	Dy2-O2	2.353(9)	Dy3-O5^{i}	2.352(9)
Dy1-O1^{i}	2.323(9)	Dy2-O12	2.389(11)	Dy3-O8	2.394(10)
Dy1-O3	2.328(9)	Dy2-O5^{i}	2.403(9)	Dy3-O13^{i}	2.446(9)
Dy1-O13	2.427(9)	Dy2-O3	2.448(9)	Dy3-N2	2.492(10)
Dy1-N6	2.494(13)	Dy2-N4	2.532(11)	Dy3-O11	2.505(12)
Dy2-O5	2.313(9)	Dy3-O2	2.295(10)		
Bond angles (°)					
O4-Dy1-O14	84.5(4)	O6-Dy2-O2	101.6(3)	O2-Dy3-O5^{i}	71.9(3)
O4-Dy1-O7	98.2(4)	O5-Dy2-O12	136.1(4)	O10-Dy3-O5^{i}	83.7(3)
O14-Dy1-O7	87.0(4)	O13-Dy2-O12	80.1(4)	O1-Dy3-O5^{i}	132.8(3)
O4-Dy1-O1^{i}	98.9(4)	O6-Dy2-O12	71.6(4)	O2-Dy3-O8	109.2(4)
O14-Dy1-O1^{i}	95.4(4)	O2-Dy2-O12	105.4(4)	O10-Dy3-O8	72.2(4)
O7-Dy1-O1^{i}	162.9(3)	O5-Dy2-O5^{i}	70.4(4)	O1-Dy3-O8	81.2(4)
O4-Dy1-O3	137.0(4)	O13-Dy2-O5^{i}	91.9(3)	O5^{i}-Dy3-O8	137.4(4)
O14-Dy1-O3	138.3(4)	O6-Dy2-O5^{i}	140.3(3)	O2-Dy3-O13^{i}	77.3(3)
O7-Dy1-O3	83.1(3)	O2-Dy2-O5^{i}	70.0(3)	O10-Dy3-O13^{i}	120.9(4)
O1^{i}-Dy1-O3	83.9(3)	O12-Dy2-O5^{i}	73.6(4)	O1-Dy3-O13^{i}	71.9(3)
O4-Dy1-O13	158.6(3)	O5-Dy2-O3	77.4(3)	O5^{i}-Dy3-O13^{i}	74.1(3)
O14-Dy1-O13	77.4(4)	O13-Dy2-O3	62.2(3)	O8-Dy3-O13^{i}	148.4(3)
O7-Dy1-O13	92.0(3)	O6-Dy2-O3	74.5(3)	O2-Dy3-N2	63.1(3)
O1^{i}-Dy1-O13	72.1(3)	O2-Dy2-O3	126.0(3)	O10-Dy3-N2	143.8(3)
O3-Dy1-O13	62.6(3)	O12-Dy2-O3	122.6(4)	O1-Dy3-N2	72.4(3)
O4-Dy1-N6	72.7(4)	O5^{i}-Dy2-O3	142.6(3)	O5^{i}-Dy3-N2	132.1(3)
O14-Dy1-N6	156.4(4)	O5-Dy2-N4	78.8(3)	O8-Dy3-N2	75.7(4)
O7-Dy1-N6	90.4(4)	O13-Dy2-N4	124.2(3)	O13^{i}-Dy3-N2	80.6(3)
O1^{i}-Dy1-N6	94.0(4)	O6-Dy2-N4	77.8(3)	O2-Dy3-O11	68.9(4)
O3-Dy1-N6	64.4(4)	O2-Dy2-N4	62.8(3)	O10-Dy3-O11	79.2(4)
O13-Dy1-N6	126.2(3)	O12-Dy2-N4	144.2(4)	O1-Dy3-O11	150.7(4)
O5-Dy2-O13	77.0(3)	O5^{i}-Dy2-N4	125.0(3)	O5^{i}-Dy3-O11	71.2(4)

O5-Dy2-O6	149.2(3)	O3-Dy2-N4	63.9(3)	O8-Dy3-O11	70.2(4)
O13-Dy2-O6	100.3(3)	O2-Dy3-O10	144.5(4)	O13^{i}-Dy3-O11	137.3(4)
O5-Dy2-O2	85.0(3)	O2-Dy3-O1	129.0(3)	N2-Dy3-O11	105.2(4)
O13-Dy2-O2	158.0(3)	O10-Dy3-O1	86.5(4)		

Table S3. Selected bond lengths (Å) and angles (°) of cluster **HNP**–**Dy$_6$**.

Bond lengths (Å)					
Dy1-O6	2.261(14)	Dy2-O3	2.329(11)	Dy3-O4	2.199(14)
Dy1-O2	2.337(12)	Dy2-O2	2.348(11)	Dy3-O3	2.365(12)
Dy1-O1	2.348(13)	Dy2-O10	2.357(11)	Dy3-O9	2.374(11)
Dy1-O9^{i}	2.363(13)	Dy2-O9	2.373(12)	Dy3-O7^{i}	2.381(16)
Dy1-O8	2.39(2)	Dy2-O11	2.391(12)	Dy3-O12	2.424(15)
Dy1-O5	2.400(16)	Dy2-O10^{i}	2.400(11)	Dy3-O1^{i}	2.462(12)
Dy1-N1	2.468(16)	Dy2-O13	2.411(15)	Dy3-O14	2.47(2)
Dy1-O10^{i}	2.475(11)	Dy2-N3	2.542(14)	Dy3-N5	2.510(17)
Bond angles (°)					
O6-Dy1-O2	148.4(4)	O3-Dy2-O2	127.1(4)	O4-Dy3-O3	134.4(5)
O6-Dy1-O1	77.6(5)	O3-Dy2-O10	119.5(4)	O4-Dy3-O9	151.1(5)
O2-Dy1-O1	121.3(5)	O2-Dy2-O10	104.5(4)	O3-Dy3-O9	73.0(4)
O6-Dy1-O9^{i}	76.5(5)	O3-Dy2-O9	73.6(4)	O4-Dy3-O7^{i}	90.7(6)
O2-Dy1-O9^{i}	85.6(4)	O2-Dy2-O9	153.6(4)	O3-Dy3-O7^{i}	77.4(5)
O1-Dy1-O9^{i}	71.5(4)	O10-Dy2-O9	71.2(4)	O9-Dy3-O7^{i}	107.1(5)
O6-Dy1-O8	102.4(7)	O3-Dy2-O11	77.4(4)	O4-Dy3-O12	98.8(6)
O2-Dy1-O8	76.5(7)	O2-Dy2-O11	89.7(5)	O3-Dy3-O12	73.5(5)
O1-Dy1-O8	145.6(6)	O10-Dy2-O11	137.6(4)	O9-Dy3-O12	78.7(5)
O9^{i}-Dy1-O8	142.6(6)	O9-Dy2-O11	78.5(4)	O7^{i}-Dy3-O12	147.1(5)
O6-Dy1-O5	79.4(6)	O3-Dy2-O10^{i}	148.0(4)	O4-Dy3-O1^{i}	94.8(5)
O2-Dy1-O5	126.6(5)	O2-Dy2-O10^{i}	70.6(4)	O3-Dy3-O1^{i}	122.9(4)
O1-Dy1-O5	78.6(6)	O10-Dy2-O10^{i}	71.6(5)	O9-Dy3-O1^{i}	69.3(4)
O9^{i}-Dy1-O5	144.9(5)	O9-Dy2-O10^{i}	83.5(4)	O7^{i}-Dy3-O1^{i}	74.7(5)
O8-Dy1-O5	67.8(7)	O11-Dy2-O10^{i}	76.3(4)	O12-Dy3-O1^{i}	135.0(5)
O6-Dy1-N1	145.4(5)	O3-Dy2-O13	84.2(4)	O4-Dy3-O14	75.9(7)
O2-Dy1-N1	64.9(4)	O2-Dy2-O13	81.7(5)	O3-Dy3-O14	135.4(7)

O1-Dy1-N1	71.5(5)	O10-Dy2-O13	73.3(4)	O9-Dy3-O14	76.4(6)
O9^{i}-Dy1-N1	107.2(5)	O9-Dy2-O13	119.9(5)	O7^{i}-Dy3-O14	143.5(7)
O8-Dy1-N1	94.7(6)	O11-Dy2-O13	149.0(4)	O12-Dy3-O14	69.3(7)
O5-Dy1-N1	79.6(5)	O10^{i}-Dy2-O13	127.3(4)	O1^{i}-Dy3-O14	72.8(7)
O6-Dy1-O10^{i}	79.8(5)	O3-Dy2-N3	63.8(4)	O4-Dy3-N5	70.5(5)
O2-Dy1-O10^{i}	69.5(4)	O2-Dy2-N3	63.3(4)	O3-Dy3-N5	63.9(4)
O1-Dy1-O10^{i}	138.2(4)	O10-Dy2-N3	143.4(4)	O9-Dy3-N5	135.2(4)
O9^{i}-Dy1-O10^{i}	69.3(4)	O9-Dy2-N3	135.0(4)	O7^{i}-Dy3-N5	75.5(5)
O8-Dy1-O10^{i}	73.6(6)	O11-Dy2-N3	78.6(5)	O12-Dy3-N5	78.2(6)
O5-Dy1-O10^{i}	130.4(5)	O10^{i}-Dy2-N3	127.0(4)	O1^{i}-Dy3-N5	146.4(5)
N1-Dy1-O10^{i}	134.4(4)	O13-Dy2-N3	70.8(5)	O14-Dy3-N5	128.3(7)

Table S4. *SHAPE* analysis of the Dy(III) in cluster **Dy$_6$**.

Label	**Shape**	**Symmetry**	**Distortion** (°) **Dy1**
OP-8	D_{8h}	Octagon	44.094
HPY-8	C_{7v}	Heptagonal pyramid	35.496
HBPY-8	D_{6h}	Hexagonal bipyramid	31.256
CU-8	O_h	Cube	28.991
SAPR-8	D_{4d}	Square antiprism	23.468
TDD-8	D_{2d}	Triangular dodecahedron	24.673
JGBF-8	D_{2d}	Johnson-Gyrobifastigium (J26)	29.886
JETBPY-8	D_{3h}	Johnson-Elongated triangular bipyramid (J14)	39.795
JBTP-8	C_{2v}	Johnson-Biaugmented trigonal prism (J50)	22.900
BTPR-8	C_{2v}	Biaugmen tedtrigonal prism	24.299
JSD-8	D_{2d}	Snub disphenoid (J84)	23.867
TT-8	T_d	Triakis tetrahedron	27.667
ETBPY-8	D_{3h}	Elongated trigonal bipyramid	36.830

Label	**Shape**	**Symmetry**	**Distortion** (°) **Dy2**
OP-8	D_{8h}	Octagon	47.368
HPY-8	C_{7v}	Heptagonal pyramid	36.884
HBPY-8	D_{6h}	Hexagonal bipyramid	28.688
CU-8	O_h	Cube	30.401
SAPR-8	D_{4d}	Square antiprism	27.441
TDD-8	D_{2d}	Triangular dodecahedron	26.497
JGBF-8	D_{2d}	Johnson-Gyrobifastigium (J26)	26.688
JETBPY-8	D_{3h}	Johnson-Elongated triangular bipyramid (J14)	38.847
JBTP-8	C_{2v}	Johnson-Biaugmented trigonal prism (J50)	26.540

BTPR-8	C_{2v}	Biaugmen tedtrigonal prism	26.281
JSD-8	D_{2d}	Snub disphenoid (J84)	29.186
TT-8	T_d	Triakis tetrahedron	29.269
ETBPY-8	D_{3h}	Elongated trigonal bipyramid	38.782

Label	**Shape**	**Symmetry**	**Distortion** (°) **Dy3**
HP-7	D_{7h}	Heptagon	45.496
HPY-7	C_{6v}	Heptagonal pyramid	27.104
PBPY-7	D_{5h}	Pentagonal bipyramid	26.955
COC-7	C_{3v}	Capped octahedron	29.777
CTPR-7	C_{2v}	Capped trigonal prism	28.888
JPBPY-7	D_{5h}	Johnson pentagonal bipyramid (J13)	22.080
JETPY-7	C_{3v}	Elongated triangular pyramid (J7)	36.682

Table S5. *SHAPE* analysis of the Dy(III) in cluster **HNP**–**Dy$_6$**.

Label	**Shape**	**Symmetry**	**Distortion** (°) **Dy1**
OP-8	D_{8h}	Octagon	45.913
HPY-8	C_{7v}	Heptagonal pyramid	37.158
HBPY-8	D_{6h}	Hexagonal bipyramid	32.223
CU-8	O_h	Cube	32.187
SAPR-8	D_{4d}	Square antiprism	25.393
TDD-8	D_{2d}	Triangular dodecahedron	24.985
JGBF-8	D_{2d}	Johnson-Gyrobifastigium (J26)	32.585
JETBPY-8	D_{3h}	Johnson-Elongated triangular bipyramid (J14)	41.206
JBTP-8	C_{2v}	Johnson-Biaugmented trigonal prism (J50)	23.531
BTPR-8	C_{2v}	Biaugmen tedtrigonal prism	25.056
JSD-8	D_{2d}	Snub disphenoid (J84)	24.709
TT-8	T_d	Triakis tetrahedron	30.668
ETBPY-8	D_{3h}	Elongated trigonal bipyramid	39.882

Label	**Shape**	**Symmetry**	**Distortion** (°) **Dy2**
OP-8	D_{8h}	Octagon	44.072
HPY-8	C_{7v}	Heptagonal pyramid	35.389
HBPY-8	D_{6h}	Hexagonal bipyramid	29.866
CU-8	O_h	Cube	30.321
SAPR-8	D_{4d}	Square antiprism	26.024
TDD-8	D_{2d}	Triangular dodecahedron	25.248
JGBF-8	D_{2d}	Johnson-Gyrobifastigium (J26)	27.258
JETBPY-8	D_{3h}	Johnson-Elongated triangular bipyramid (J14)	40.005
JBTP-8	C_{2v}	Johnson-Biaugmented trigonal prism (J50)	25.637

BTPR-8	C_{2v}	Biaugmen tedtrigonal prism	24.601
JSD-8	D_{2d}	Snub disphenoid (J84)	26.990
TT-8	T_d	Triakis tetrahedron	29.241
ETBPY-8	D_{3h}	Elongated trigonal bipyramid	37.982

Label	**Shape**	**Symmetry**	**Distortion** (°) **Dy3**
OP-8	D_{8h}	Octagon	47.810
HPY-8	C_{7v}	Heptagonal pyramid	36.974
HBPY-8	D_{6h}	Hexagonal bipyramid	33.740
CU-8	O_h	Cube	30.782
SAPR-8	D_{4d}	Square antiprism	25.697
TDD-8	D_{2d}	Triangular dodecahedron	25.391
JGBF-8	D_{2d}	Johnson-Gyrobifastigium (J26)	31.608
JETBPY-8	D_{3h}	Johnson-Elongated triangular bipyramid (J14)	40.035
JBTP-8	C_{2v}	Johnson-Biaugmented trigonal prism (J50)	25.885
BTPR-8	C_{2v}	Biaugmen tedtrigonal prism	26.108
JSD-8	D_{2d}	Snub disphenoid (J84)	26.906
TT-8	T_d	Triakis tetrahedron	29.643
ETBPY-8	D_{3h}	Elongated trigonal bipyramid	38.557

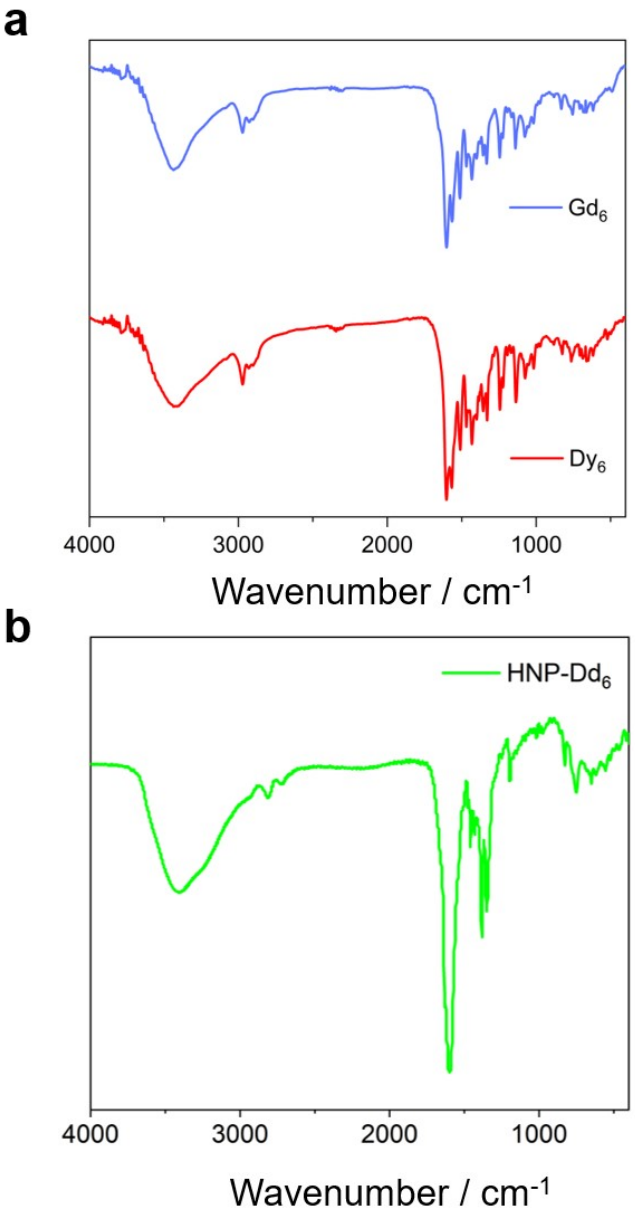

Figure S1. Infrared spectra (IR) of clusters **Dy_6**, **Gd_6** (a) and **HNP–Dy_6** (b).

Fourier transform infrared absorption spectroscopy (FT-IR) results indicated that the absorption peaks of **Dy_6** are mainly located at 3429, 2970, 1600, 1565, 1432, 1136 cm^{-1}, respectively. The absorption peak at around 3429 cm^{-1} cans be attributed to the stretching vibration of ν(HO–H) in the H_2O molecule. The peak around 2970 cm^{-1} can be attributed to the stretching vibration of $-CH_3$. The strong peaks around 1600 cm^{-1} and 1565 cm^{-1} can be attributed to the C=N stretching vibration of the imine group (–C=N–). The peak around 1432 cm^{-1} can be attributed to the stretching vibration of the aromatic ring C=N and C=C. The strong absorption peak around 1136 cm^{-1} can be attributed to the strong vibration between the alcoholic hydroxyl groups C–O in the ligand. The infrared (IR, cm^{-1})

absorption spectrum of **Gd_6** clusters is similar to that of **Dy_6**, and its absorption peaks are mainly located at 3429, 2970, 1601, 1568, 1431, 1138 cm^{-1}, respectively. The absorption peak around 3429 cm^{-1} cans be attributed to the stretching vibration of ν(HO–H) in the H_2O molecule. The peak around 2970 cm^{-1} can be attributed to the stretching vibration of $-CH_3$. The strong peaks around 1601 cm^{-1} and 1568 cm^{-1} can be attributed to the C=N stretching vibration of the imine group (–C=N–). The peak around 1431 cm^{-1} can be attributed to the stretching vibration of the aromatic ring C=N and C=C. The strong absorption peak around 1138 cm^{-1} can be attributed to the strong vibration between the alcoholic hydroxyl groups C–O in the ligand. For **HNP-Dy_6**, the FT-IR absorption peaks are mainly located at 3429, 1601, 1384, 1350, 1200 cm^{-1}, respectively. The absorption peak around 3429 cm^{-1} cans be attributed to the stretching vibration of ν(HO–H) in the H_2O molecule. The strong peak around 1601 cm^{-1} can be attributed to the C=N stretching vibration of the imine group (–C=N–). The peaks around 1384 cm^{-1} and 1350 cm^{-1} can be attributed to the bending vibration of $-CH_3$. The strong absorption peak around 1200 cm^{-1} can be attributed to the strong vibration between the alcoholic hydroxyl groups C–O in the ligand.

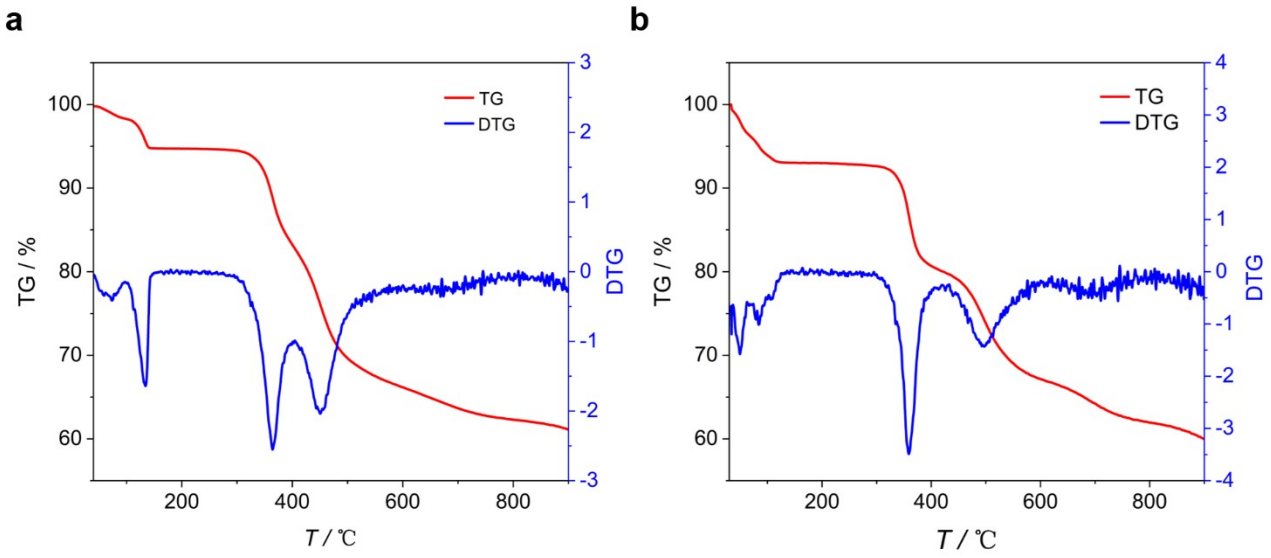

Figure S2. TG curve of **Dy_6** (a) and **HNP–Dy_6** (b).

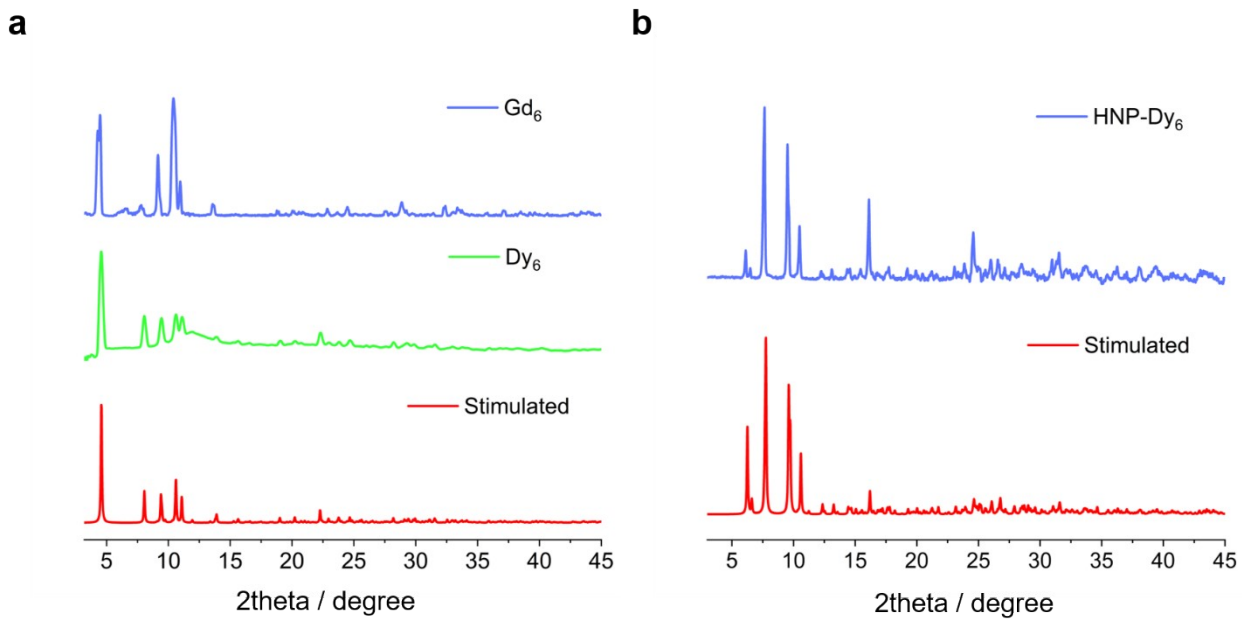

Figure S3. Powder diffraction pattern (PXRD) of clusters **Dy_6**, **Gd_6** (a) and **HNP**–**Dy_6** (b).

Table S6. Major species assigned in the HRESI-MS of **Dy_6** in positive mode.

Fragments	*Calc. m/z*	*Exp. m/z*
(a) $[Dy_6(L^1)_2(O)_4(OH)_4(CH_3OH)_3(H_2O)_2]^{2+}$	1163.59	1163.54
(b) $[Dy_6(L^1)_2(O)_4(CH_3COO)_2(OH)_2(CH_3OH)_2]^{2+}$	1172.58	1172.55
(c) $[Dy_6(L^1)_2(O)_4(CH_3COO)_2(OH)_2(CH_3OH)_2(H_2O)]^{2+}$	1181.09	1181.08
(d) $[Dy_6(L^1)_2(O)_4(OH)_4(DMF)_2(CH_3OH)]^{2+}$	1188.10	1188.08
(e) $[Dy_6(L^1)_2(O)_4(CH_3COO)_4(OH)(H_2O)_3]^{+}$	2435.17	2435.16
(f) $[Dy_6(L^1)_2(O)_4(CH_3COO)_5(DMF)(H_2O)]^{+}$	2513.20	2513.18
(g) $[Dy_6(L^1)_2(O)_4(CH_3COO)_4(OH)(DMF)(CH_3OH)_2(H_2O)_3]^{+}$	2572.26	2572.22

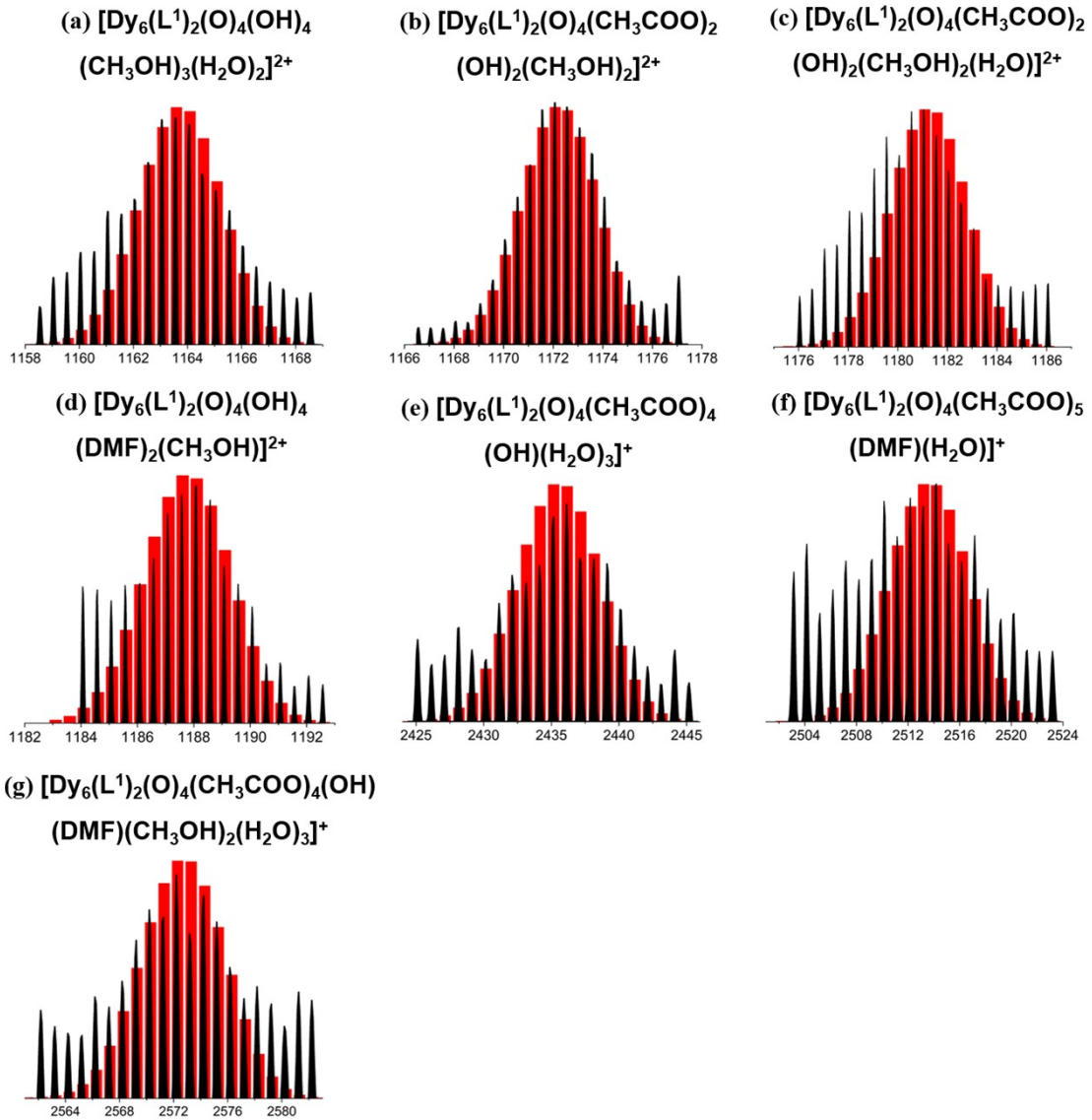

Figure S4. The superposed simulated and observed spectra of several species for cluster **Dy_6**.

Table S7. Major species assigned in the HRESI-MS of **HNP–Dy$_6$** in positive mode.

Fragments	*Calc. m/z*	*Exp. m/z*
(a) $[Dy_6(L^2)_2(O)_4(CH_3COO)_2(CH_3O)(OH)_2(H_2O)_2]^+$	2261.91	2261.87
(b) $[Dy_6(L^2)_2(O)_4(CH_3COO)_2(CH_3O)_3(CH_3OH)(H_2O)]^+$	2302.96	2302.89
(c) $[Dy_6(L^2)_2(O)_4(CH_3COO)_2(CH_3O)_3(CH_3OH)(H_2O)_2]^+$	2321.97	2321.89
(d) $[Dy_6(L^2)_2(O)_4(CH_3COO)_4(CH_3O)(CH_3OH)(H_2O)_2]^+$	2375.96	2375.94
(e) $[Dy_6(L^2)_2(O)_4(CH_3COO)_4(CH_3O)(CH_3OH)_5(H_2O)_5]^+$	2560.09	2560.02
(f) $[Dy_6(L^2)_2(O)_4(CH_3COO)_4(CH_3O)(CH_3OH)_5(H_2O)_6]^+$	2576.10	2576.04

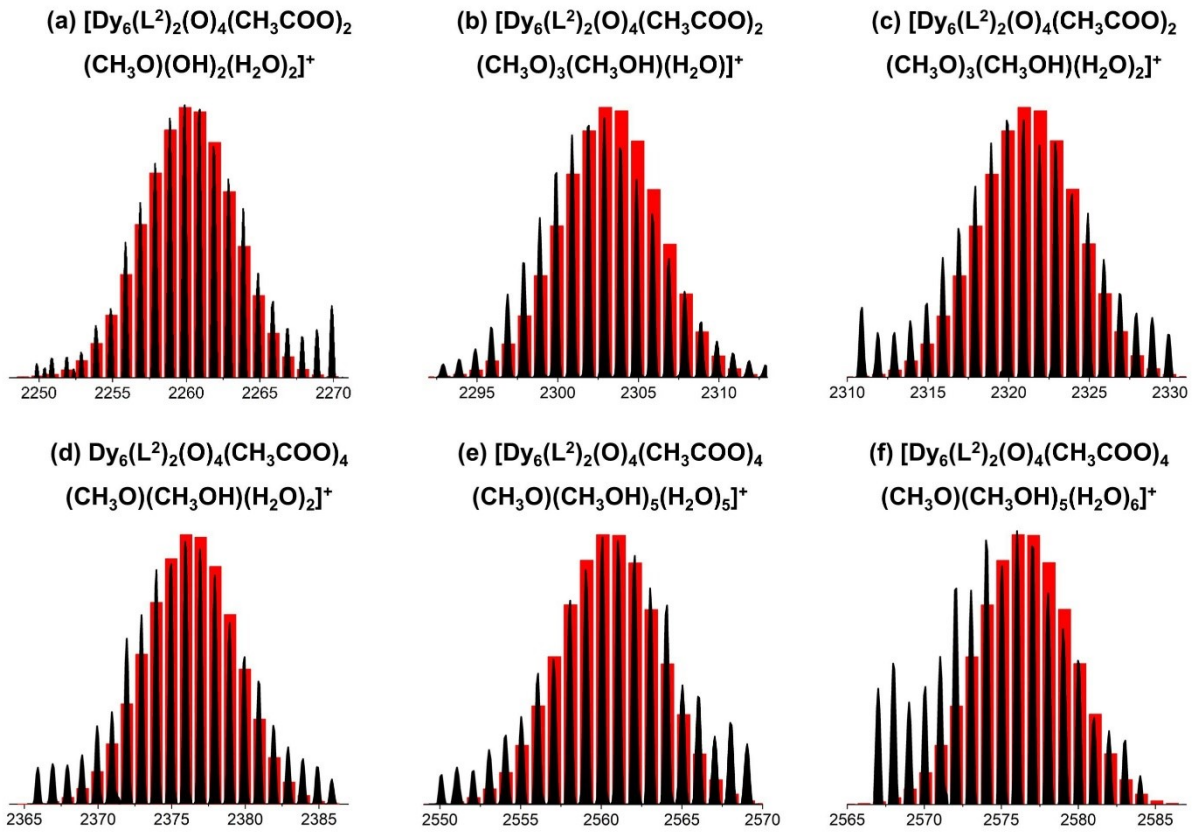

Figure S5. The superposed simulated and observed spectra of several species for cluster **HNP–Dy$_6$**.

Table S8. Major species assigned in the HRESI-MS of **Dy_6** with different in-source CID (0–100 eV) in positive mode.

Fragments	*Calc. m/z*	*Exp. m/z*
(a) $[Dy_6(L^1)_2(O)_4(OH)_4(H_2O)_5]^{2+}$	1142.57	1142.55
(b) $[Dy_6(L^1)_2(O)_4(OH)_4(CH_3OH)_3(H_2O)_2]^{2+}$	1163.59	1163.56
(c) $[Dy_6(L^1)_2(O)_4(CH_3COO)_2(OH)_3(CH_3OH)(H_2O)_4]^{2+}$	1199.58	1199.58
(d) $[Dy_6(L^1)_2(O)_4(CH_3COO)_2(OH)_3(CH_3OH)(H_2O)_5]^{+}$	1209.59	1209.54
(e) $[Dy_6(L^1)_2(O)_4(CH_3COO)_4(OH)(H_2O)_3]^{+}$	2435.16	2435.17
(f) $[Dy_6(L^1)_2(O)_4(CH_3COO)_5(H_2O)_3]^{+}$	2478.17	2478.20
(g) $[Dy_6(L^1)_2(O)_4(CH_3COO)_5(DMF)]^{+}$	2495.19	2495.20

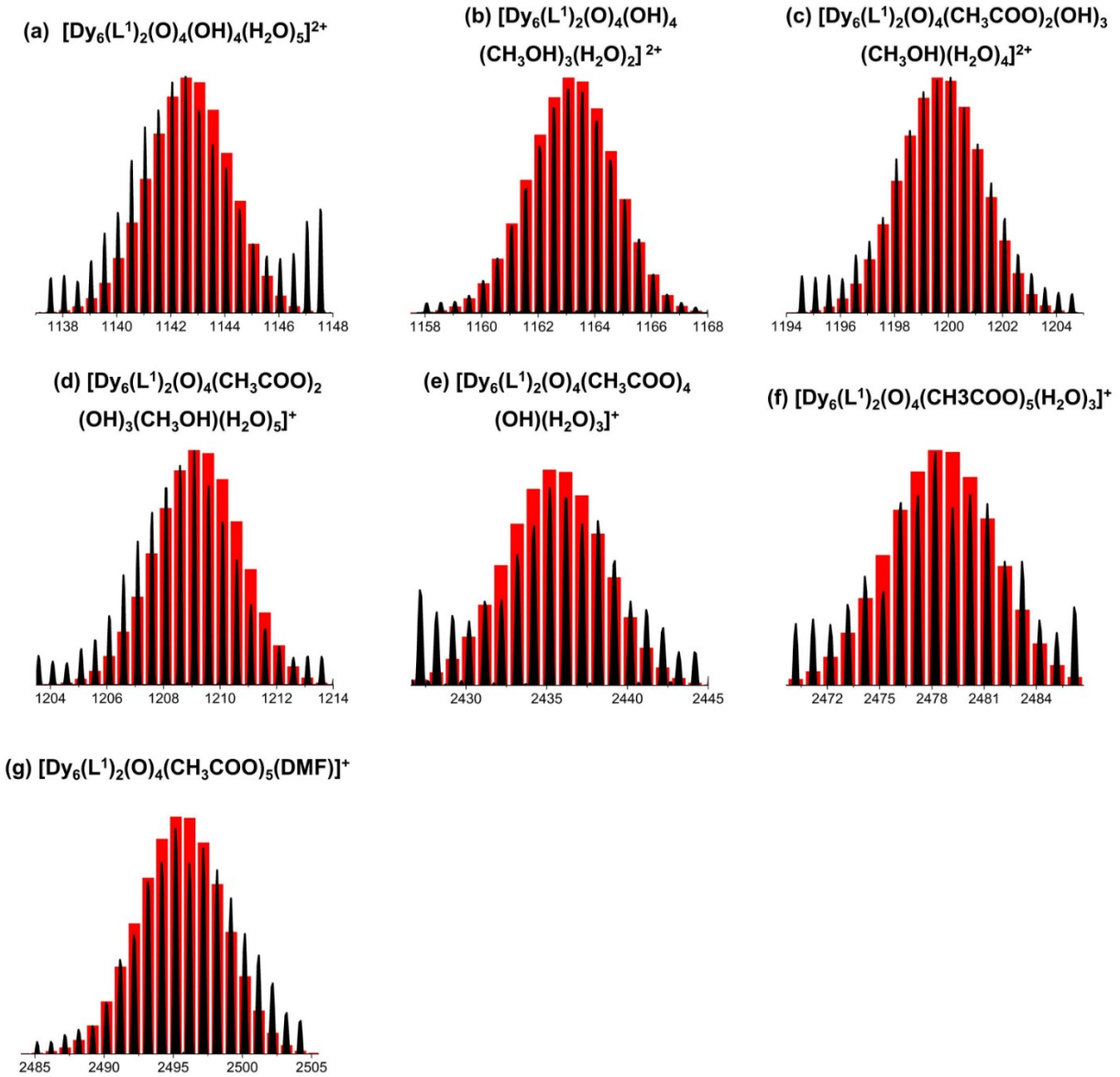

Figure S6. The superposed simulated and observed spectra of several species for **Dy_6** with different in-source CID (0–100 eV).

Table S9. Major species assigned in the HRESI-MS of **HNP-Dy$_6$** with different in-source CID (0–100 eV) in positive mode.

Fragments	*Calc. m/z*	*Exp. m/z*
(a) $[Dy_6(L^2)_2(O)_4(CH_3COO)(CH_3O)_4(H_2O)_2]^+$	2259.94	2259.87
(b) $[Dy_6(L^2)_2(O)_4(CH_3O)_3(OH)_2(CH_3OH)_3(H_2O)_2]^+$	2302.00	2301.89
(c) $[Dy_6(L^2)_2(O)_4(CH_3O)_3(OH)_2(DMF)(CH_3OH)_3(H_2O)_2]^+$	2374.05	2373.95
(d) $[Dy_6(L^2)_2(O)_4(CH_3COO)_2(CH_3O)_3(DMF)_2(CH_3OH)(H_2O)_3]^+$	2485.08	2485.00
(e) $[Dy_6(L^2)_2(O)_4(CH_3COO)_4(CH_3O)(CH_3OH)_5(H_2O)_5]^+$	2560.09	2560.04
(f) $[Dy_6(L^2)_2(O)_4(CH_3COO)_3(CH_3O)_2(CH_3OH)_6(H_2O)_5]^+$	2562.12	2562.02

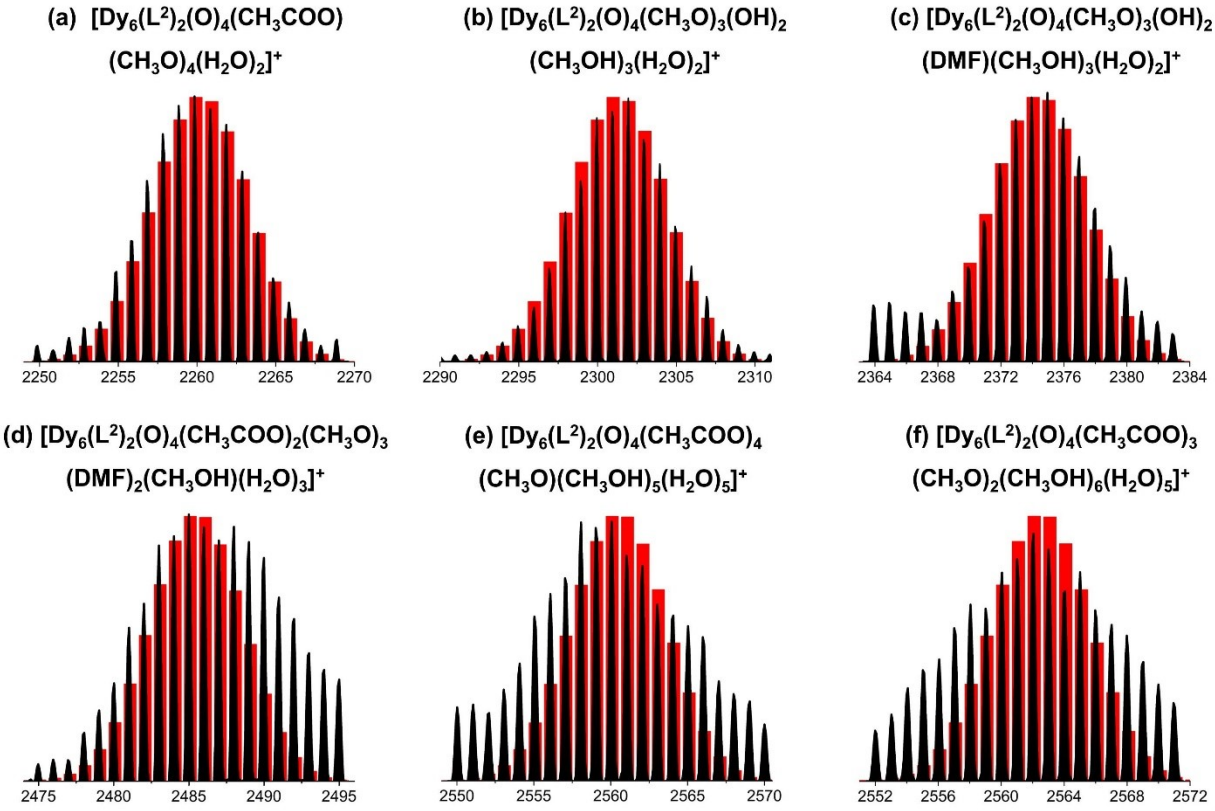

Figure S7. The superposed simulated and observed spectra of several species for **HNP–Dy$_6$** with different in-source CID (0–100 eV).

Table S10.Major species assigned in the Time-dependent HRESI-MS of **Dy_6** in positive mode.

Fragments	*Calc. m/z*	*Exp. m/z*
$[Dy_2(L^1)(OH)_2(DMF)_8(CH_3OH)_6(H_2O)_4]^{2+}$	877.38	877.49
$[Dy_2(L^1)(OH)_2(DMF)_8(CH_3OH)_5(H_2O)_6]^{2+}$	878.37	878.48
$[Dy_2(L^1)(OH)_2(DMF)_8(CH_3OH)_8(H_2O)_2]^{2+}$	891.40	891.50
$[Dy_3(L^1)(OH)_6(DMF)(H_2O)_2]^{+}$	1242.13	1242.03
$[Dy_3(L^1)(OH)_6(CH_3OH)_2(H_2O)_2]^{+}$	1265.16	1265.08
$[Dy_3(L^1)(OH)_6(DMF)_2(CH_3OH)_2]^{+}$	1345.07	1345.23
$[Dy_3(L^1)(OH)_6(DMF)_2(CH_3OH)_2(H_2O)_4]^{+}$	1416.26	1416.14
$[Dy_6(L^1)_2(O)_4(CH_3COO)(OH)_3(CH_3OH)_2]^{2+}$	1151.58	1151.53
$[Dy_6(L^1)_2(O)_4(OH)_4(CH_3OH)_3(H_2O)_2]^{2+}$	1163.59	1163.54
$[Dy_6(L^1)_2(O)_4(CH_3COO)_2(OH)_2(CH_3OH)_2]^{2+}$	1172.58	1172.55
$[Dy_6(L^1)_2(O)_4(CH_3COO)_2(OH)_2(CH_3OH)_2(H_2O)]^{2+}$	1181.09	1181.08
$[Dy_6(L^1)_2(O)_4(OH)_4(DMF)_2(CH_3OH)]^{2+}$	1188.10	1188.08
$[Dy_6(L^1)_2(O)_4(CH_3COO)_5(DMF)]^{+}$	2496.21	2496.20
$[Dy_6(L^1)_2(O)_4(CH_3COO)_5(DMF)(H_2O)]^{+}$	2513.20	2513.18
$[Dy_6(L^1)_2(O)_4(CH_3COO)_4(OH)(DMF)(CH_3OH)_2(H_2O)_3]^{+}$	2572.26	2572.22

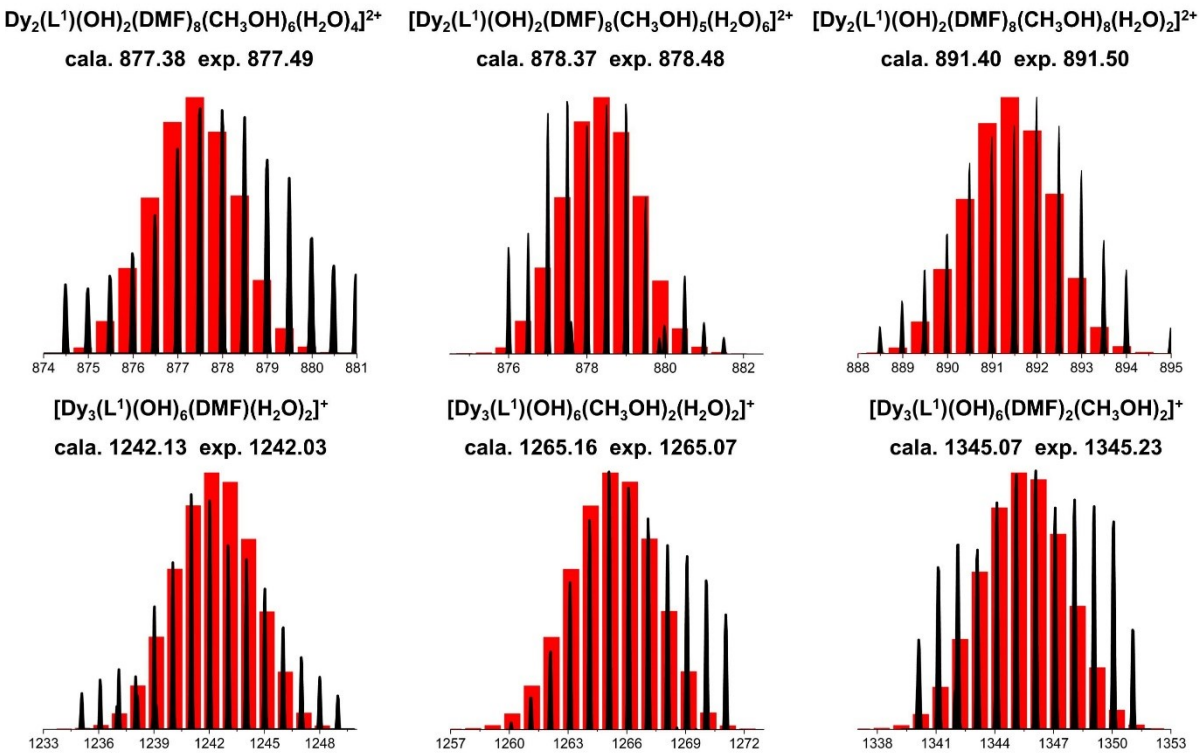

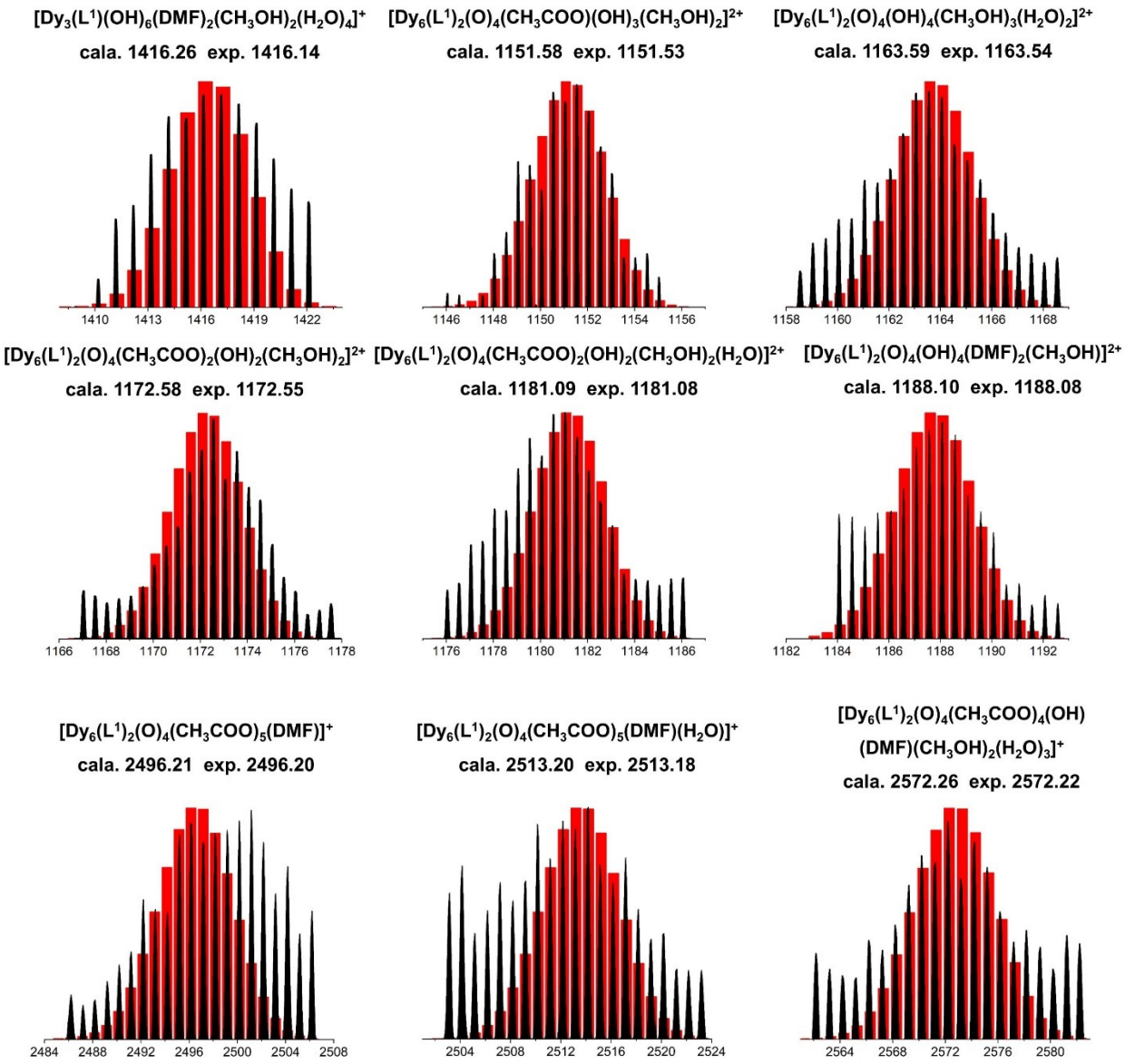

Figure S8. Time-dependent HRESI-MS spectra for the assembly of **Dy_6** in positive mode.

Table S11.Major species assigned in the Time-dependent HRESI-MS of **HNP-Dy$_6$** in positive mode.

Fragments	*Calc. m/z*	*Exp. m/z*
$[Dy_2(L^2)(CH_3O)_2(OH)(H_2O)]^+$	925.16	925.03
$[Dy_2(L^2)(CH_3O)_2(OH)(CH_3OH)(H_2O)_4]^+$	1009.10	1008.93
$[Dy_2(L^2)(OH)_3(DMF)_2(CH_3OH)(H_2O)]^+$	1071.14	1070.96
$[Dy_3(L^2)(OH)_6(DMF)_3(CH_3OH)]^+$	1342.13	1342.08
$[Dy_3(L^2)(OH)_6(DMF)(CH_3OH)_3(H_2O)_6]^+$	1370.16	1370.07
$[Dy_3(L^2)(OH)_6(DMF)(CH_3OH)_4(H_2O)_2]^+$	1448.22	1448.08
$[Dy_3(L^2)(OH)_6(DMF)_2(CH_3OH)_5(H_2O)_7]^+$	1524.26	1524.10
$[Dy_5(L^2)_2(O)_4(OH)_2]^+$	1919.95	1919.98
$[Dy_5(L^2)_2(O)_4(OH)_2(CH_3OH)]^+$	1946.94	1946.96
$[Dy_5(L^2)_2(O)_4(OH)_2(CH_3OH)(H_2O)]^+$	1967.98	1967.96
$[Dy_6(L^2)_2(O)_4(CH_3COO)_2(CH_3O)(OH)_2(H_2O)_2]^+$	2261.91	2261.87
$[Dy_6(L^2)_2(O)_4(CH_3COO)_2(CH_3O)_3(CH_3OH)(H_2O)]^+$	2302.96	2302.87
$[Dy_6(L^2)_2(O)_4(CH_3COO)_2(CH_3O)_3(CH_3OH)(H_2O)_2]^+$	2321.97	2321.89
$[Dy_6(L^2)_2(O)_4(CH_3COO)_4(CH_3O)(CH_3OH)(H_2O)_2]^+$	2375.96	2375.94
$[Dy_6(L^2)_2(O)_4(CH_3COO)_4(CH_3O)(CH_3OH)_5(H_2O)_5]^+$	2560.09	2560.02
$[Dy_6(L^2)_2(O)_4(CH_3COO)_4(CH_3O)(CH_3OH)_5(H_2O)_6]^+$	2576.10	2576.04

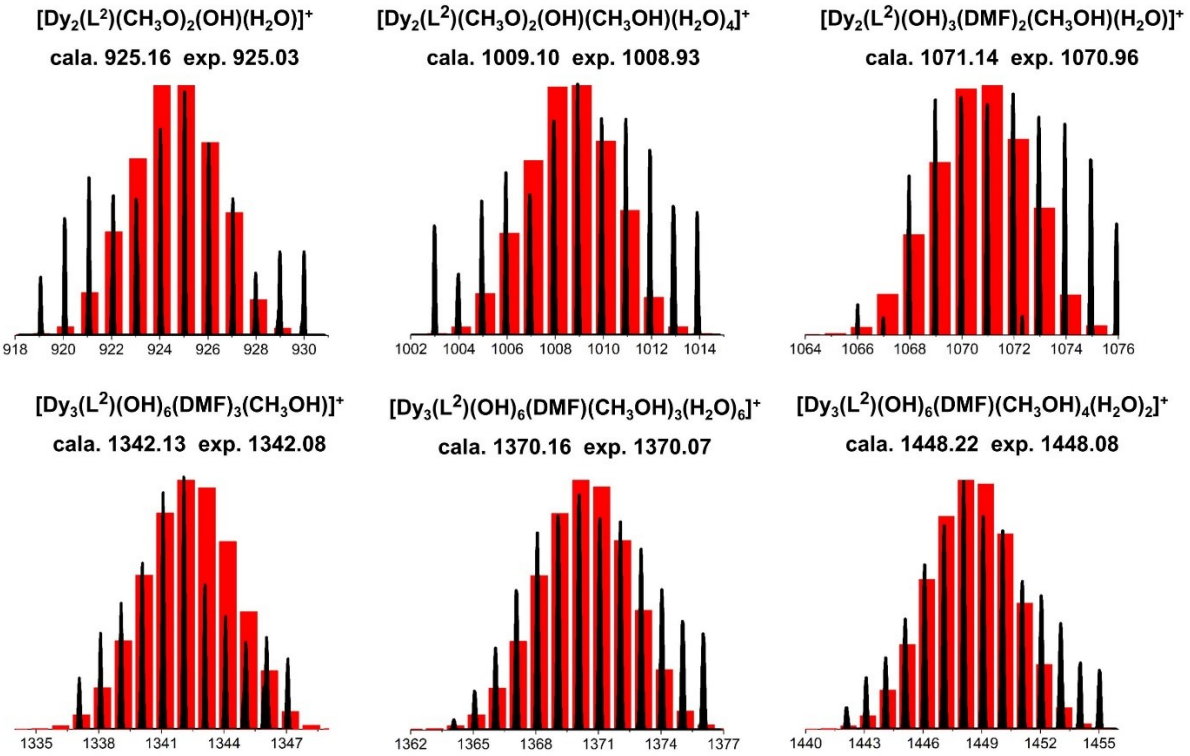

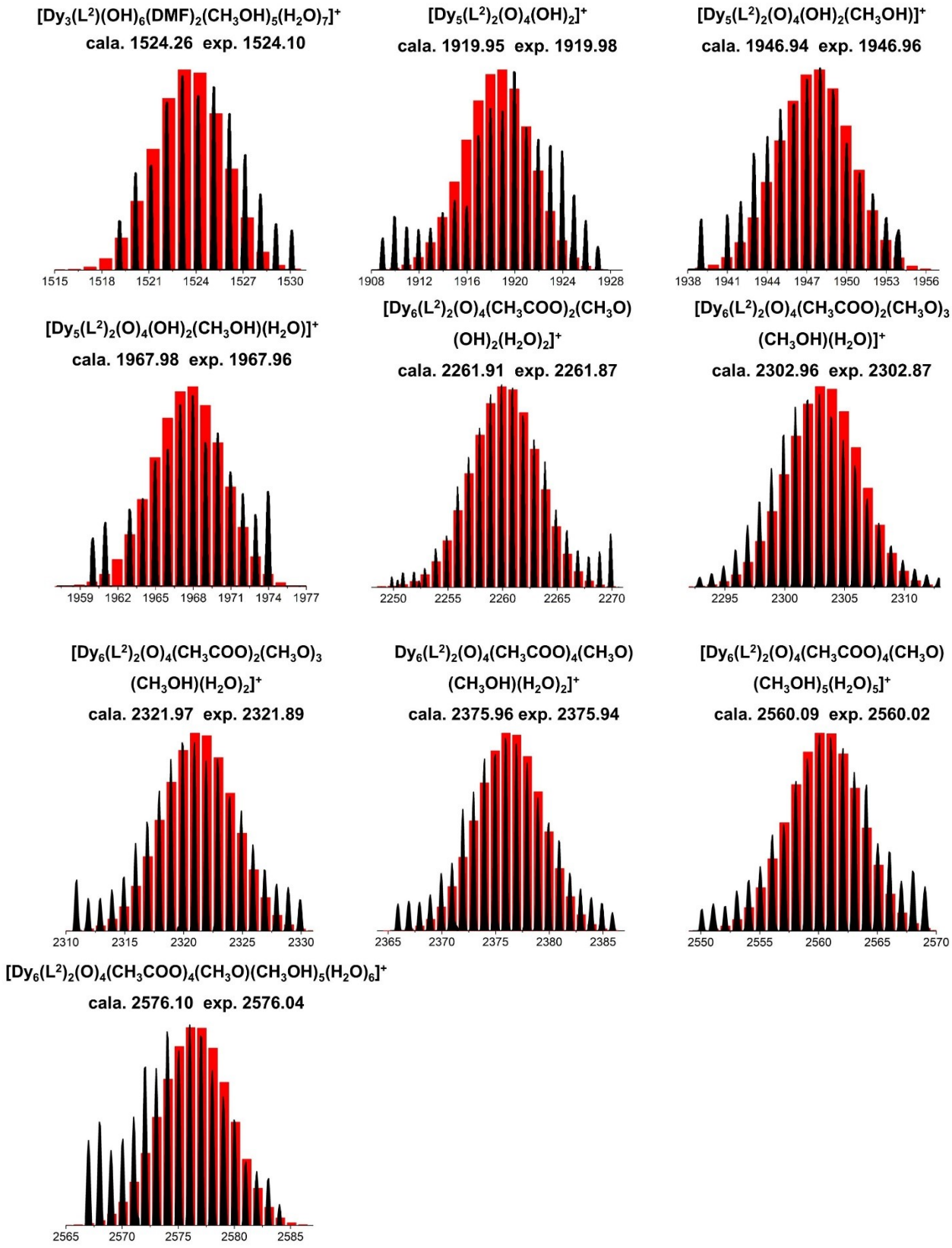

Figure S9. Time-dependent HRESI-MS spectra for the assembly of **HNP**–**Dy$_6$** in positive mode.

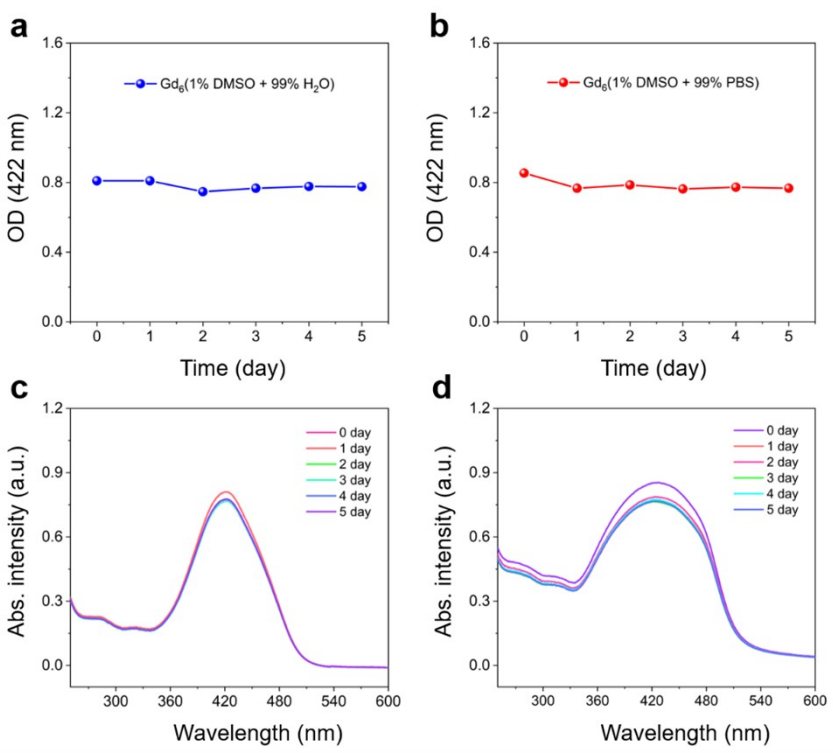

Figure S10. Stability of **Gd_6** dispersed in (a) H_2O and (b) PBS for 5 days, UV-Vis absorption spectra of **Gd_6** in (c) H_2O and (d) PBS.

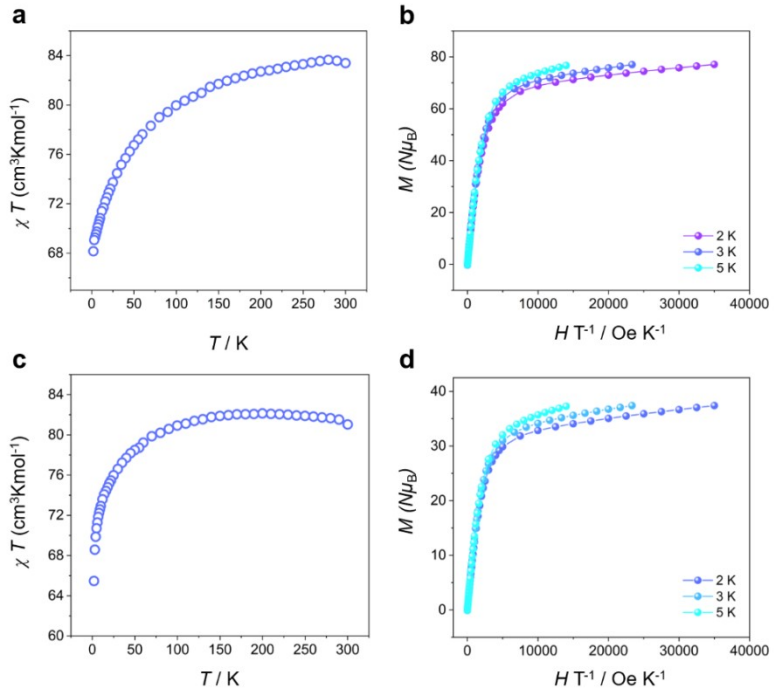

Figure S11. Temperature dependence of $\chi_m T$ for (a) **Dy_6** and (c) **HNP-Dy_6**, *M* vs. *H*/*T* plots of (b) **Dy_6** and (d) **HNP**–**Dy_6**.

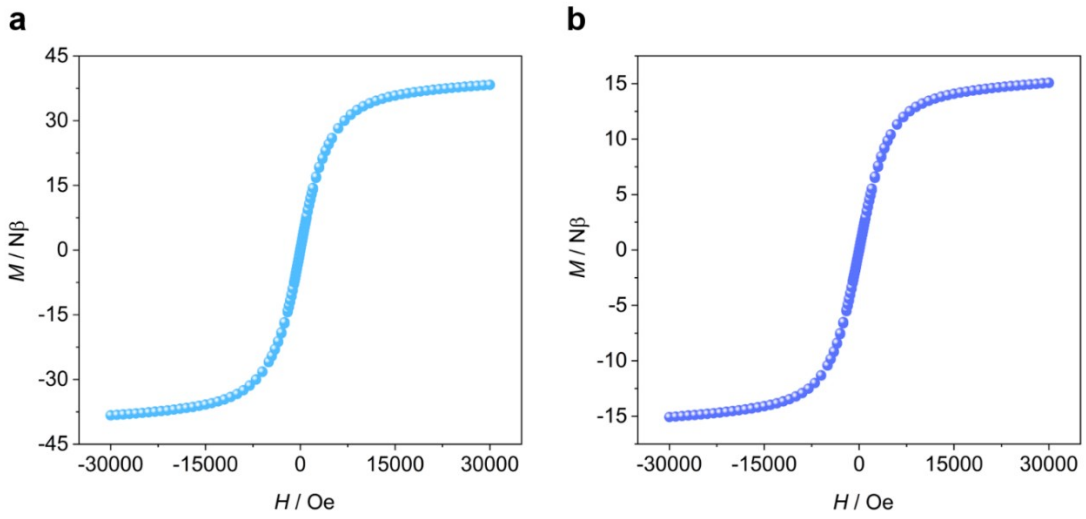

Figure S12. Loop curve graph of **Dy_6** (a) and **HNP–Dy_6** (b) at 2 K.

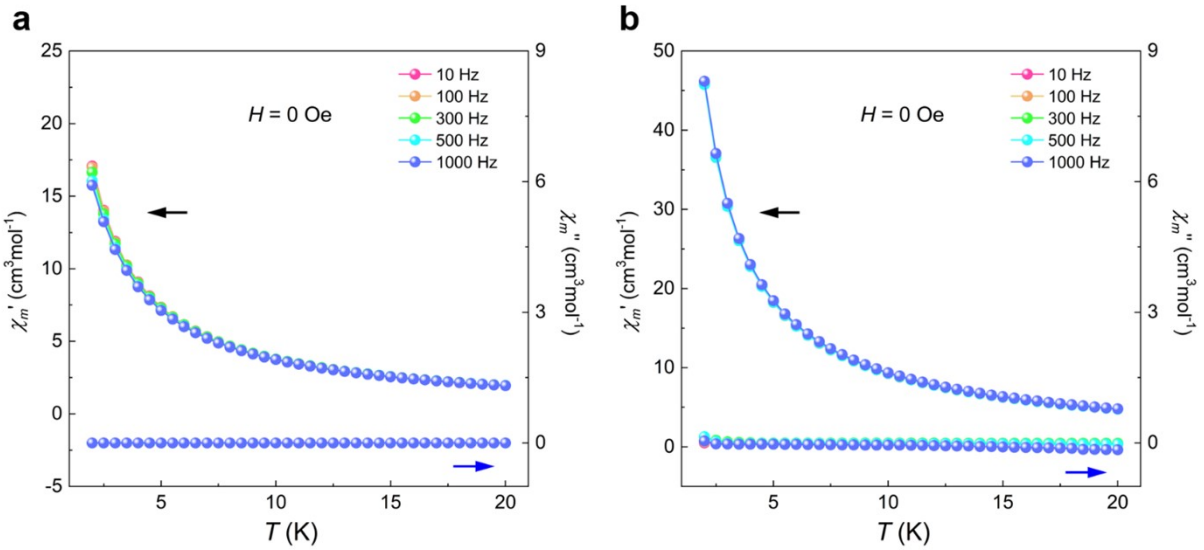

Figure S13. Temperature dependence of the real (χ') and imaginary (χ'') ac susceptibilities at different frequencies in the 0 Oe dc fields for **Dy_6** (a) and **HNP–Dy_6** (b).

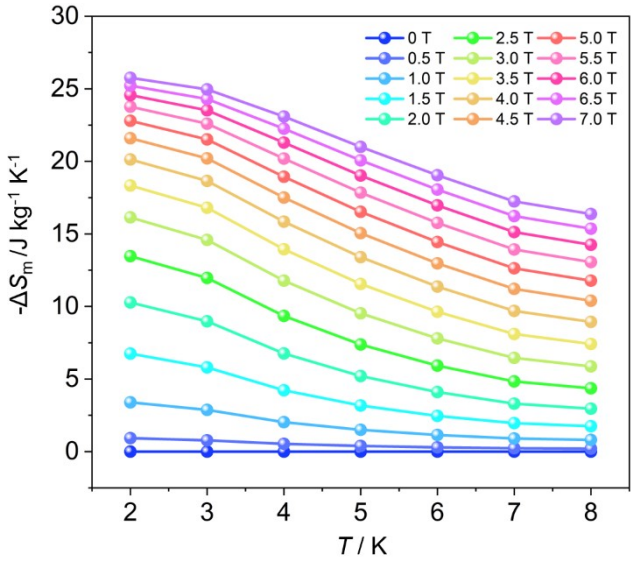

Figure S14. Magnetic entropy change (-ΔS_m) of **Gd_6** at different temperatures (2–8 K) and magnetic fields (0–7 T).